Influence of longitudinal strain on the critical current of Nb_3Sn strands

Xi Feng Lu, Steve Pragnell and Damian P. Hampshire

Superconductivity Group, Physics Department,

Durham University, Durham DH1 3LE, UK

Contract. No.: EFDA/06-1534

FU06-CT—2006-00469

Final Report

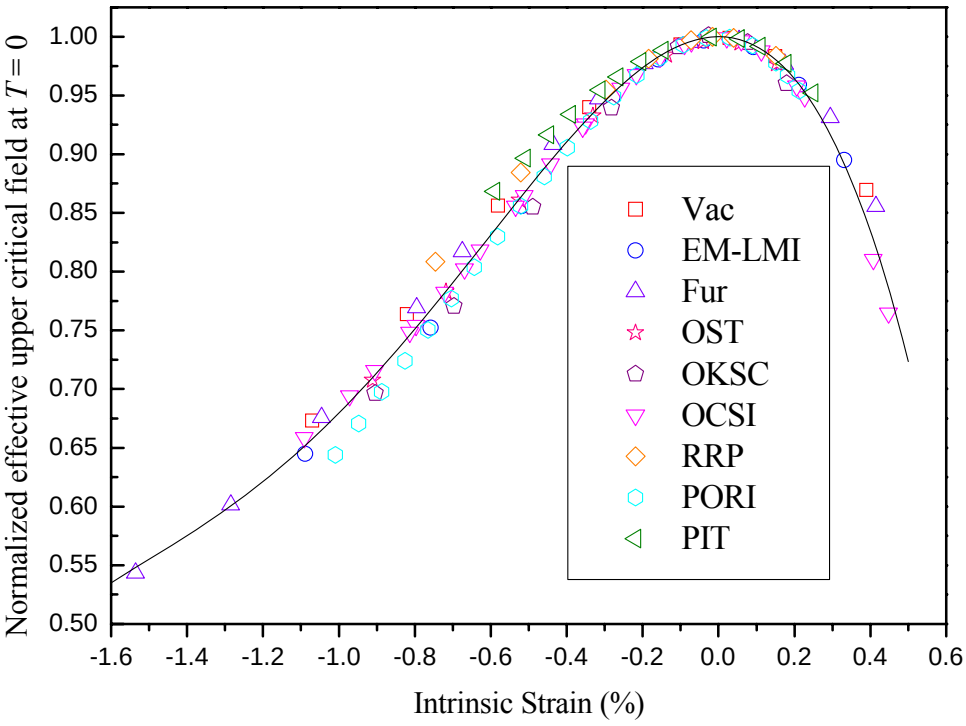

The normalized effective upper critical field at $T = 0$ as a function of intrinsic strain for the powder-in-tube SMI-PIT strand and the advanced PORI strand, compared with previous data for seven other doped Nb_3Sn strands

Completed Oct 2008

Durham University

ACKNOWLEDGEMENTS

The authors acknowledge the help and support of E. Salpietro, A. Vostner and E. Mossang.

We also acknowledge the many discussions we have had with those in the EFDA and ITER community including: R. Zanino, D. Bessette, L. Bottura, D. Bruzzone, N. Cheggour, J. Duchateau, J. Ekin, W. H. Fietz, H. Fillunger, A. Godeke, P. Komarek, R. Maix, N. Martovetsky, N. Mitchell, J. Minervini, A. Nyilas, A. Nijhuis, A. Portone, K. Osamura, L. Savoldi Richard, and J. Schultz.

Durham University

TABLE OF CONTENTS

Durham University

EXTENDED ABSTRACT

Comprehensive measurements are reported of the engineering critical current density ($J_C(B,T,\varepsilon)$) at 10 μVm^{-1} and $n(B,T,\varepsilon)$ over the range 10 – 100 μVm^{-1} as a function of magnetic field, temperature and uniaxial strain. The scope of this report contains three parts:

i) Measurements of $J_C(B,T,\varepsilon)$ and $n(B,T,\varepsilon)$ on a Shapemetal Innovation (SMI) PIT Nb_3Sn strand. $J_C(B,T,\varepsilon)$ data of the SMI-PIT strand are accurately described by the Durham scaling law with nine free-parameters which was proposed previously and derived using microscopic and phenomenological theoretical analysis. The relationship between the *n*-value and critical current (I_C) is parameterised using a modified power law of the form $n = 1+rI_C^s$, where *r* and *s* are approximately constant. The critical current density and *n*-value of the PIT strand is very high and the normalised strain dependence of $J_C(B,T,\varepsilon)$ and $n(B,T,\varepsilon)$ is similar to other Nb_3Sn strands.

ii) Measurements of $J_C(B,T,\varepsilon)$ and $n(B,T,\varepsilon)$ on a Luvata PORI Nb_3Sn strand. Although the short heat-treatment means that J_C (and I_C) is significantly (~ 40%) lower than the optimised values achieved in other advanced strands, the normalised strain dependence of $J_C(B,T,\varepsilon)$ and $n(B,T,\varepsilon)$ is similar to other Nb_3Sn strands. $J_C(B,T,\varepsilon)$ data of the PORI strand can be accurately parameterized using a standard scaling law with 9 free-parameters. It is also demonstrated that the $J_C(B,T,\varepsilon)$ data can be parameterised by just 6 free parameters by assuming that the strain dependence of the normalized effective upper critical field is similar for all advanced internal-tin strands. Hence the results presented here on a low J_C strand provide evidence that the 6 free parameter scaling law can be used to accurately characterize other advanced internal-tin Nb_3Sn strands with a wide range of heat-treatments and I_C.

Accompanying this report are two spreadsheets that contain tabulations of the J_C and *n*-value data, as well as the scaling-law parameterisation of $J_C(B,T,\varepsilon)$ and $n(B,T,\varepsilon)$ for SMI-PIT and PORI strands respectively at : http://www.dur.ac.uk/superconductivity.durham/publications.html

iii) Compressive strain cycling results are presented on the same rod-restack-process (RRP) strand investigated in a previous report (EFDA/05-1296) that considered reversibility limits in both tensile and compressive strain. The strong sensitivity of these strands to tensile strain has now been confirmed by other groups and is now considered a property specific to this type of Nb_3Sn strand. In contrast to our previous results, no damage was observed in these measurements for compressive strains down to -1 %. The different behaviour in the strand may be due to inhomogeneity in the strand, better handling, sample variations associated with pre-existing cracks (which have been observed in RRP strands elsewhere using electron microscopy)

or use of rectangular Cu-Be sample holders rather than Tee-shaped Ti-alloy when measuring this particular strand.

For the PIT strand:

p	q	n	v	w	u	ε_M (%)
1.1753	2.655	***2.500***	***1.500***	***2.200***	***0***	0.020
$A(0)$ ($Am^{-2}T^{3-n}K^{-2}$)	$T_C^*(0)$ (K)	$B_{C2}^*(0,0)$ (T)	c_2	c_3	c_4	
1.356×10^8	17.47	29.46	–0.6153	–0.5780	–0.3002	

Table II: Durham scaling law parameters for the SMI-PIT strand derived from variable strain, field and temperature data using 9 free-parameters. Data were obtained at 4.2, 8, 10, 12 and 14 K. The four parameters in bold were not varied in the fitting procedure. (RMS ~ 3.2 A)

p	q	C	C_{a1}	C_{a2}
2.149	4.520	1.233×10^{12}	60.9422	25.0876
$\varepsilon_{0,a}$ (%)	ε_M (%)	$B_{C20max}^*(0,0)$ (T)		$T_{C0max}^*(0)$ (K)
0.4069	0.0193	34.10		17.04

Table IV: The official ITER scaling parameters for the SMI-PIT strand derived from variable field, variable temperature and variable strain data – 9 free parameters. Data fitting was limited to 4.2, 8, 10, 12 and 14 K. (RMS ~ 4.1 A)

For the PORI strand:

Universal Values	c_2	c_3	c_4	n	v	w	u
	-0.77462	***-0.59345***	***-0.13925***	***2.5***	***1.50***	***2.20***	***0***
$A(0)$ ($Am^{-2}T^{3-n}K^{-2}$)	$T_C^*(0)$ (K)	$B_{C2}^*(0,0)$ (T)	p	q	ε_M (%)		
3.644×10^7	16.63	30.01	1.0129	2.653	0.1044		

Table VI. Durham scaling law parameters for the PORI strand with 6 free parameters. Data were obtained at 4.2, 6, 8, 10, 12 and 14 K. The seven parameters whose values are given in bold were not varied in the fitting procedure. (RMS ~ 3.1 A)

p	q	C	C_{a1}	C_{a2}
0.4077	1.828	2.128×10^{10}	57.3785	12.9486
$\varepsilon_{0,a}$ (%)	ε_{M} (%)	$B^{*}_{C20max}(0,0)$ (T)		$T^{*}_{C0max}(0)$ (K)
0.2377	0.0917	30.00		16.02

Table IX: The official ITER scaling parameters for the PORI strand derived from variable field, variable temperature and variable strain data – 9 free parameters. Data obtained at 4.2, 6, 8, 10, 12 and 14 K were used in the fitting. (RMS ~ 3.1 A)

The RMS values show that the $J_C(B,T,\varepsilon)$ data is most accurately described using a 9 free-parameter Durham Scaling law. A comparison between the two fits to the data at 4.2 K is shown in figure 10. The Durham law includes a term in $1/\kappa^2$ which is consistent with experiment data[1] computational work [2] and theory[3] (rather than the $1/\kappa$ term proposed in the 2008 ITER scaling law).

IPR REPORT

The important results from the task are summarised in the extended abstract and summarised in detail in the accompanying report – there was no IPR created in the course of this work .

Pre-existing knowledge is outlined in the publicly available literature – in particular the published reports and articles of those scientists cited in the reference section of this report.

There is no foreground IPR – all techniques used are encompassed within the publicly available state-of-the-art literature.

There is no new business confidential information, business confidential know-how, or trade secrets - the materials used in this report were supplied without any obligations re confidentiality .

Disclosure of the information – this report will be made available through the public-accessible Web in the first instance and thereafter discussed at specialist scientific meetings and published in international scientific journals.

The work in this report has been discussed with the Technology Transfer Unit at Durham University.

Prof. Damian P. Hampshire Durham University
October 21st 2008.

1 INTRODUCTION

There are broadly four different types of Nb_3Sn strand: Bronze-route strands that have low hysteresis losses (< 200 kJm^{-3}) but the engineering J_C (defined as the critical current divided by the total cross-section area of the strand[4]) is also low, typically 250 Amm^{-2} at 4.2 K and 12 T (non-Cu J_C ~ 800 Amm^{-2})[5]; Internal-tin strands of which there are two types - advanced strands with J_C values of ~ 400 Amm^{-2} and losses of ~ 750 kJm^{-3} (non-Cu J_C ~ 800 Amm^{-2} - acceptable for ITER) and restack-rod-process (RRP) strands for high-energy-physics where engineering J_C values of ~1200 Amm^{-2} (non-Cu J_C ~ 900 - 1200 Amm^{-2}) have now been obtained but with very high losses; and finally powder-in-tube (PIT) strands [6] which have similar J_C values to those found in RRP strands (non-Cu J_C ~ 2500 Amm^{-2})[5,7]. The four types of strands are shown in Fig. 1 where J_C (and I_C) as a function of field at 4.2 K is shown – including the SMI-PIT Nb_3Sn strand, the PORI advanced internal-tin Nb_3Sn strand and the restack-rod-process (RRP) strand that are the subject of this report.

The effect of strain on Nb_3Sn strands is very important [8] because large strains are unavoidable in large magnets. The strains can originate from the differential thermal contraction between the components of the magnets during the process of cool-down and also the large Lorentz forces produced during high-field operation. The J_C versus strain-dependence of Nb_3Sn strands has a significant impact on the design and final performance of large Cable-in-Conduit Conductors (CICC) like those used in ITER. For several years the Summers Scaling Law was widely accepted and used to describe J_C of Nb_3Sn strands. However, measurements on the Model Coil and recently developed advanced strands showed significant deviations from the functional form given by Summers, especially at high compressive strain. It has long been known that the strand layout and composition (ternary or quaternary compounds with Ta and/or Ti additions) influences the magnitude, field and temperature dependence of the critical current. It is now clear that for any conductor design, it is necessary to know the strain dependence of J_C as a function of field and temperature, if one wants to ensure reliable conductor performance predictions.

One facility capable of measuring the field (B) and strain (ε) dependence of the critical strand current at variable temperatures (T) is available here at the University of

Durham. In the framework of the European Fusion Technology programme, the University of Durham has been involved in several strand characterization tasks (e.g. EFDA contracts 02-662, 03-1126 and 05-1296), and has a lot of experience in sample preparation, testing and evaluation of the results[1]. The broad objectives of this current task are three-fold:

i) A comprehensive characterization of $J_C(B,T,\varepsilon)$ for a high energy Physics SMI-PIT Nb_3Sn strand.

ii) A comprehensive characterization of $J_C(B,T,\varepsilon)$ for an advanced internal-tin (Luvata-PORI) Nb_3Sn strand, which was heat treated using a very short schedule and as a result has a significantly lower J_C than optimised material.

iii) Compressive strain cycling results of $J_C(B,T,\varepsilon)$ on a rod-restack-process (RRP) strand that complements a previous report (EFDA/05-1296) that considered the reversibility limits in tensile and compressive strain. The RRP Dipole strand is the same strand as reported in EFDA/05-1296.

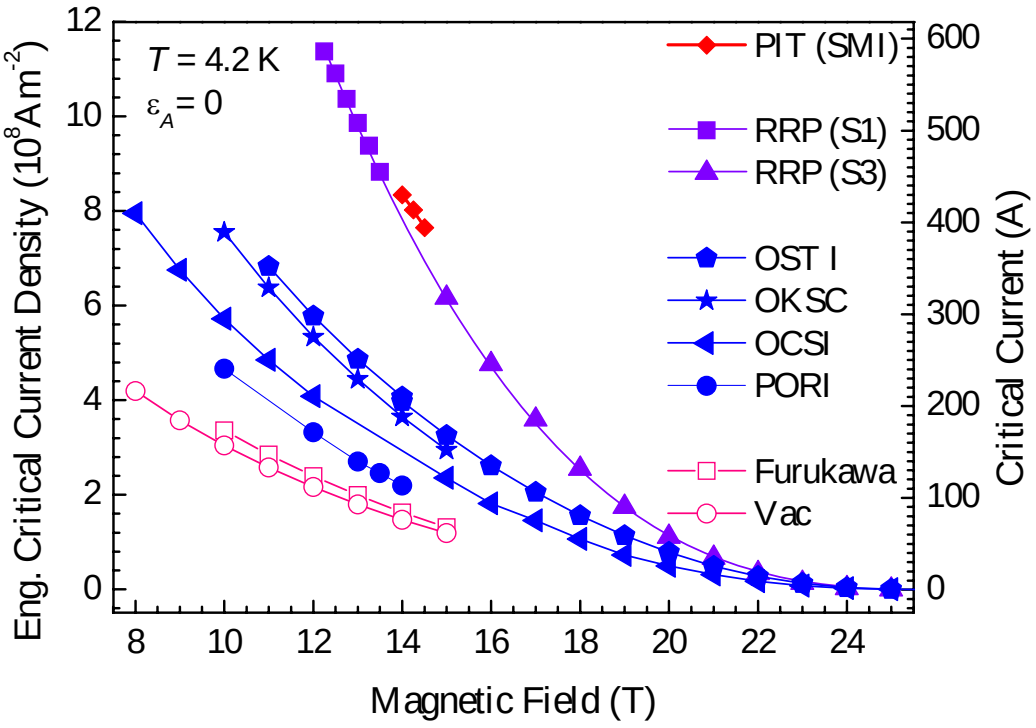

Fig. 1. Engineering critical current density J_C (and critical current I_C) versus magnetic field for Nb_3Sn strands made by different manufactures. The Vac[9] and Furukawa[10] are bronze-route strands. OST I [11], OKSC [11], OCSI [11] and PORI [12] are advanced internal-tin strands. S1 and S3 are the RRP Dipole strand[13]. PIT is the power-in-tube strand. The PIT, PORI and RRP samples are presented in this report.

The report is structured as follows: Section 2 outlines the experimental procedure. Section 3 presents the experimental results, analysis and summary for the PIT sample and the PORI sample. Sections 3.1 and 3.2 present the results. Section 3.3 presents the $J_C(B,T,\varepsilon)$ scaling-law parameterization and the parameterisation of the *n*-value data for the two strands using both Durham scaling and an ITER scaling law recently proposed for characterising Nb_3Sn strands. Section 4 presents the cycling test results on a RRP strand that investigate the reversibility limit in compressive strain. Finally, section 5 presents the summary and conclusions from these data and discusses the physical interpretation of the results.

2 EXPERIMENTAL PROCEDURE

2.1 Sample heat-treatment

Measurements were performed on chrome-plated Nb_3Sn strands 0.81 mm in diameter. All strands were heat-treated in an argon atmosphere using the heat-treatment schedules shown in Table I. They were reacted on oxidised stainless-steel mandrels in a three-zone furnace, with an additional thermocouple positioned next to the sample in order to monitor the temperature. The strands were then etched in hydrochloric acid to remove the chrome plating.

The PIT strand and the PORI strand were transferred to nickel-plated Ti–6Al–4V helical springs, to which they were attached by copper plating and soldering. The helical springs had four-turns and a T-shaped cross-section optimised to minimise the strain gradient across the strand [14,15].

For the strain cycling measurements on the RRP strand, given that the original measurements were made on Ti–6Al–4V helical springs, we chose to make measurements using a Cu-Be helical spring. The samples were attached the Cu-Be springs using copper plating and soldering. The helical springs used for these measurements have four-turns and a rectangular cross-section [14,15].

PIT strand	PORI and Dipole RRP strand
Ramp at 50° C h^{-1} to 675°C and hold for 50h	Ramp at 10°C h^{-1} to 210°C and hold for 48 h
Ramp at 50° C h^{-1} to room temperature	Ramp at 10° C h^{-1} to 400°C and hold for 48 h
	Ramp at 10° C h^{-1} to 640°C and hold for 60 h
	Ramp at 10° C h^{-1} to room temperature

Table I Heat-treatment schedules for the PIT, PORI and RRP strands.

2.2 Using the Durham $J_C(B,T,\varepsilon)$ probe

The Durham strain probe[14,16] was used to carry out voltage–current (V–I) measurements on the strands as a function of magnetic field (B), temperature (T) and applied axial strain (ε_A). The spring (and sample) is mounted onto the probe and the strain is applied by twisting the spring via concentric shafts: the inner shaft connects a worm-wheel system at the top of the probe to the top of the spring, and the outer shaft is connected to the bottom of the spring via an outer can. For measurements at 4.2 K, the outer can contains a number of holes to admit liquid helium from the surrounding bath. For measurements above 4.2 K, the outer can forms a vacuum space around the sample with a copper gasket and knife edge seal between the can and the outer shaft and the temperature is controlled via three independent pairs of Cernox thermometers and constantan wire heaters[17]. The detailed description of the experimental apparatus and techniques can be found elsewhere [4,14,16,18].

The measurements consist of monitoring the voltage across different sections of the sample as a function of the current through it. J_C (or I_C) was measured (is defined) at an electric field criterion of 10 μVm^{-1}.

3 PIT AND PORI STRANDS - RESULTS AND ANALYSIS

This report presents critical current (I_C) and engineering critical current density (J_C) data defined at an electric-field criterion of 10 μVm^{-1}, where J_C is calculated by dividing the critical current by the total cross-sectional area of the strand (5.153×10^{-7} m^2). This choice for defining an engineering J_C, rather than the often used non-Cu J_C or J_C in the superconducting layer, avoids any ambiguity or loss of clarity that can occur if the nominal value for the Cu/non-Cu ratio or the area or distribution of the reacted Nb_3Sn material in the strand is subsequently found to be significantly different from the nominal values.

3.1 PIT sample raw data

3.1.1 PIT $J_C(B,T,\varepsilon)$ data

Figure 2 shows typical electric field–current density (*E*-*J*) (and voltage–current: *V*-*I*) characteristics measured at 4.2 K and ε_A = -0.29%. The transition is sharp, indicative of the high *n*-values for the PIT strand. The noise in these measurements is a few nanovolts – primarily the Johnson noise from the room-temperature section of the voltage leads. It is clear that these characteristics are not straight lines. Nevertheless for magnet engineering purposes, it is helpful to obtain *n*-values which are calculated using the power law expression $E = \alpha J^n$ with *E* between 10 and 100 μVm^{-1}.

Figure 3a is a plot of J_C (and I_C) as a function of applied strain at 4.2 K for the PIT sample for magnetic fields at and below 14.25 T with field increments of 0.25 T. After the compressive measurements at 4.2 K had been completed, measurements were made at 8 K, 10 K and 14 K. The J_C (and I_C) data as a function of applied strain at 4.2 K and 8 K are shown in figure 3a. Figure 3b shows data taken at 10 K and 14 K (Limited data at 12 K was also measured but not shown). Figure 4 shows some reversibility data taken at 8 K – the irreversibility shown in this figure is associated with temperature variations of ± 120 mK. Nevertheless the data provide strong evidence that the strand filaments have remained undamaged throughout these measurements and that the precompression in these PIT strands is small. The engineering J_C is the highest we have measured in Durham as shown by the data shown in figure 1 taken at zero strain and by the data in figure 5 which shows the normalized I_C as a function of strain for each of the

four types of Nb_3Sn strand. In figures 3a and 3b, the solid lines were provided by the Durham scaling law and are discussed in section 3.3.

Given our experience with the RRP strand, which showed damage at strain values close to the peak in J_C (i.e. at zero intrinsic strain), we took the precaution not to risk damaging the PIT sample at 4.2 K before the variable temperature data had been measured. [13,19] As figures 3 and 4 show, this precaution was not necessary as the PIT sample is not damaged for intrinsic strains up to at least +0.25%.

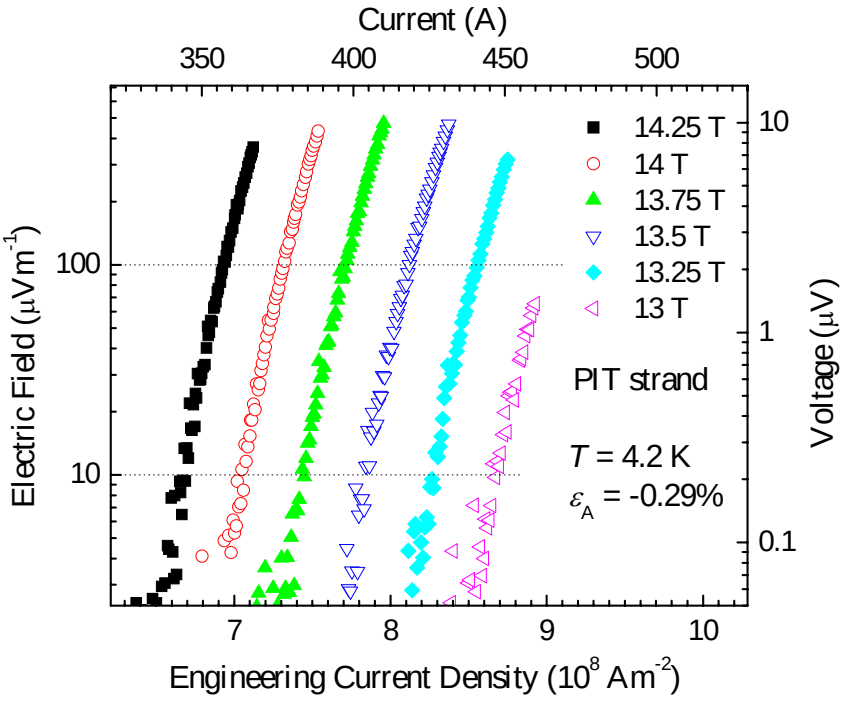

Fig. 2. Log-log plot of electric field versus engineering current density (and voltage versus current) for the SMI-PIT strand at 4.2 K, with ε_A = - 0.29% in magnetic fields between 13 T and 14.25 T in increments of 0.25 T.

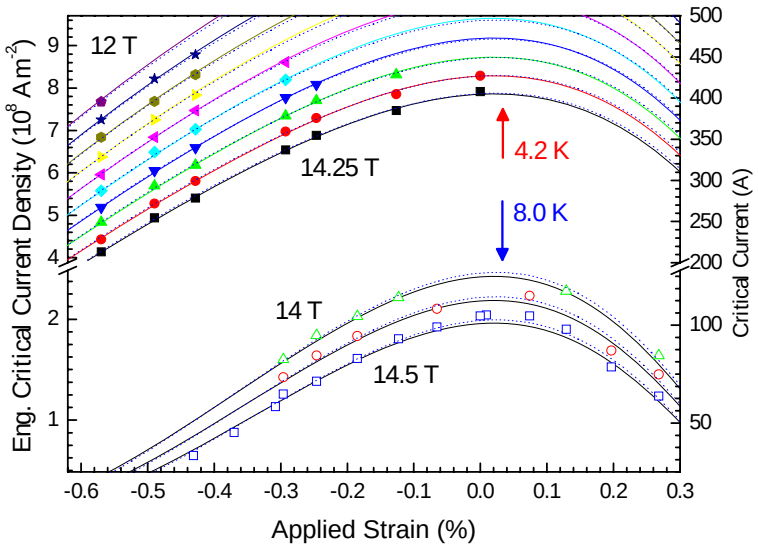

Fig. 3a. Engineering critical current density (and critical current) of SMI-PIT strand as a function of applied strain at 4.2 K in magnetic fields from 12 to 14.25 T in increments of 0.25 T and 8 K in field 14, 14.25 and 14.5 T. The solid lines are provided from fitting the 9 free-parameter Durham scaling law to all the data – the dotted lines are the scaling laws obtained from fitting the Durham 9 free-parameter scaling law to the 4.2 and 8 K data alone.[1]

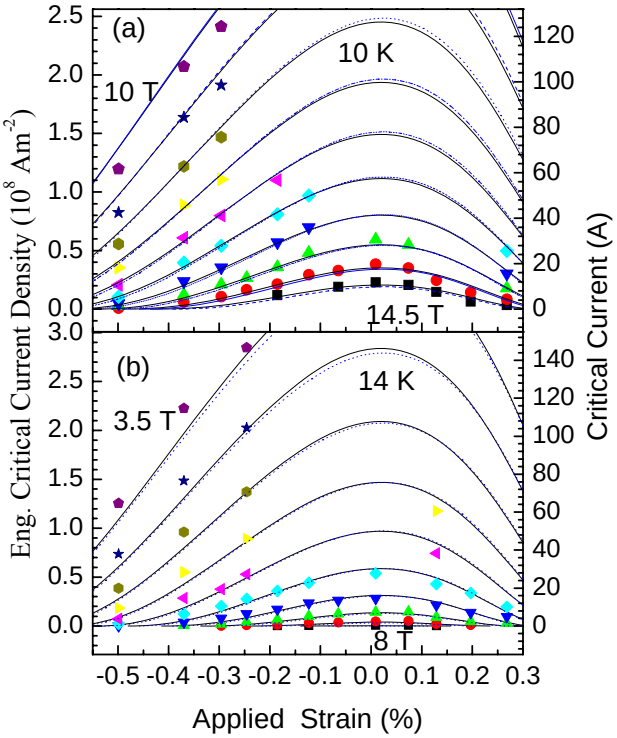

Fig. 3b. Engineering critical current density (and critical current) of SMI-PIT strand as a function of applied strain in magnetic fields (a) from 10 to 14.5 T at 10 K, and (b) from 3.5 to 8 T at 14 K. The increment of the magnetic fields is 0.5 T. The solid lines are provided from fitting the 9 free-parameter Durham scaling law to all the data – the dotted lines are the scaling laws obtained from fitting the Durham 9 free-parameter scaling law to the 4.2 and 8 K data alone.[1]

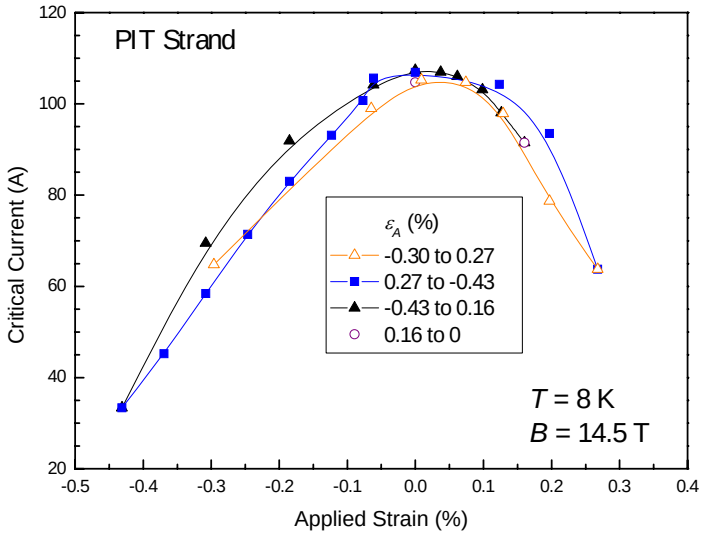

Fig. 4: The critical current as a function of applied strain in 14.5 T field at $T = 8$ K, for the SMI-PIT strand. The lines are guides to the eye.

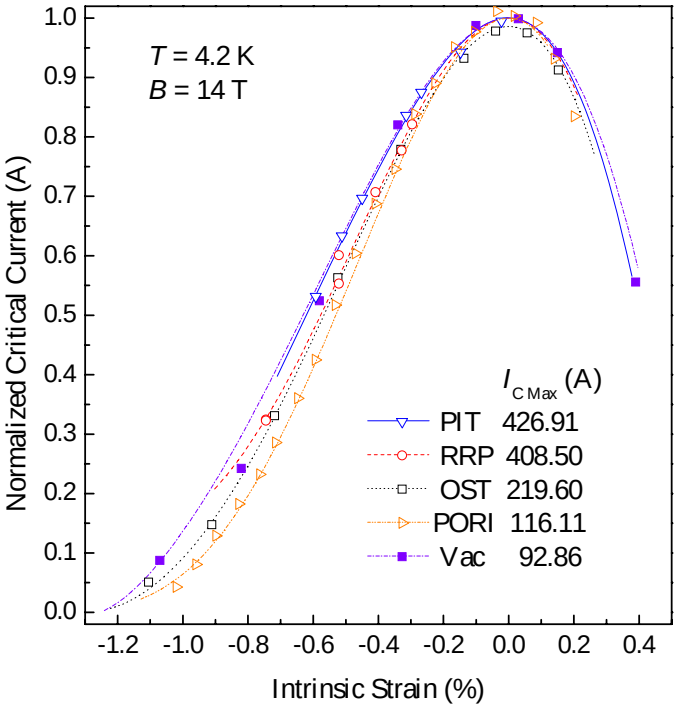

Fig. 5: Normalized critical current as a function of intrinsic strain in 14 T field at $T = 4.2$ K, for the four types of strands.

3.1.2 PIT - $n(B,T,\varepsilon)$ data

Using the power-law expression $E = \alpha J^n$ and fitting the E-J data over the range from 10 to 100 μVm^{-1}, values of n were obtained. The n-values of the PIT strand as a function of intrinsic strain ε_I are displayed in figure 6 where T = 4.2 K, B = 14 T along with other types of Nb_3Sn strands including the PORI sample. The n-values for the SMI strand are high compared to other Nb_3Sn strands (cf. fig. 6), consistent with the very sharp V-I curves. It can be seen that the strain–dependence of the n-value shows a similar inverted quasi-parabolic behaviour, similar to the critical current density, as has been observed before. In order to parameterise the relationship between the n-value and critical current, n-1 versus critical current is plotted as shown in figure 7. The straight line in figure 7 is provided by the power law shown. In fig. 8, the normalized n-value dependence shows that the different types of Nb_3Sn strand show quite similar strain behaviour as a function of intrinsic strain.

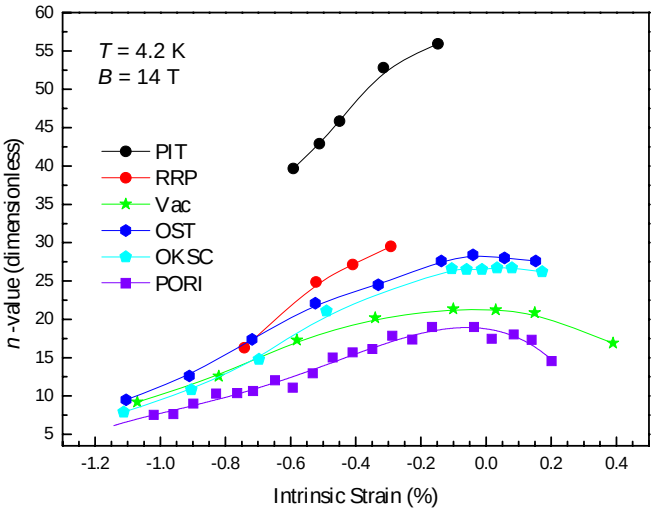

Fig. 6: n-value as a function of intrinsic strain for SMI-PIT strand compared with other strands, the PORI strand is included. All lines are guides to the eye.

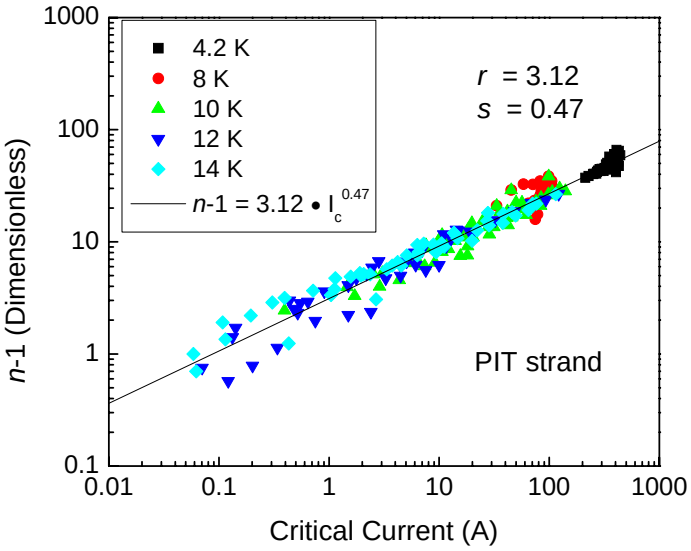

Fig. 7: The n-value obtained from fitting the experimental data to the equation $E = \alpha J^n$ over the range from 10 to 100 μVm^{-1}. Data are shown for the SMI-PIT strand plotted as n-1 as a function of critical current at T = 4.2 K, 8 K, 10 K, 12 K and 14 K in different fields. The line shows a fit to all the data using equation (9) where r = 3.12 and s = 0.47.

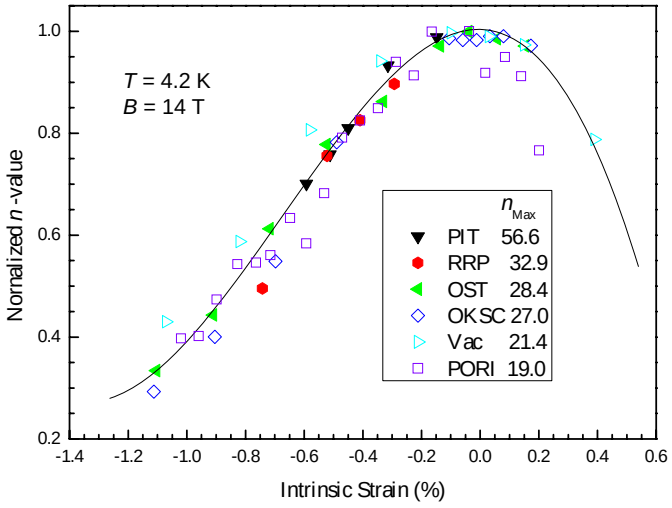

Fig. 8: Normalized n-value as a function of intrinsic strain for SMI-PIT strand compared with other strands, the PORI strand is included. The line is a guide to the eye.

3.2 PORI sample raw data

3.2.1 PORI- $J_C(B,T,\varepsilon)$ data

Figure 9 shows J_C (and I_C) of the PORI strand as a function of magnetic field from 4.2 K to 14 K with zero applied strain (ε_A =0). Figure 10 shows J_C (and I_C) as a function

of applied strain at 4.2 K in fields from 10 to 14 Tesla. These data have the well-known asymmetry in which J_C is more sensitive to the tensile strain than compressive strain. Figs 10 and 11 show the variable temperature data obtained for the PORI sample up to 12 K and fitted using a 6 free-parameter fit (Data were also taken at 14 K but are not shown).

The very short heat-treatment schedule (cf. table I) used for the PORI sample meant that J_C (and I_C) was significantly lower (~ 40% lower) than optimised values. [20] Despite the low J_C, fig. 12 shows that the normalized strain sensitivity of the critical current at 14 T and 4.2 K is broadly similar to other strands that were fabricated by the same procedure – advanced internal-tin process.

3.2.2 PORI - $n(B,T,\varepsilon)$ data

As with the PIT sample, we have used the E-J data to fit the power-law expression $E = \alpha J^n$ over the range from 10 to 100 μVm^{-1}, to obtain values of n for PORI strand. Figure 6 shows that the n value of the PORI sample is actually smaller than the Vac (bronze-route) strand, which is most probably associated with the very short heat-treatment time and low critical current.

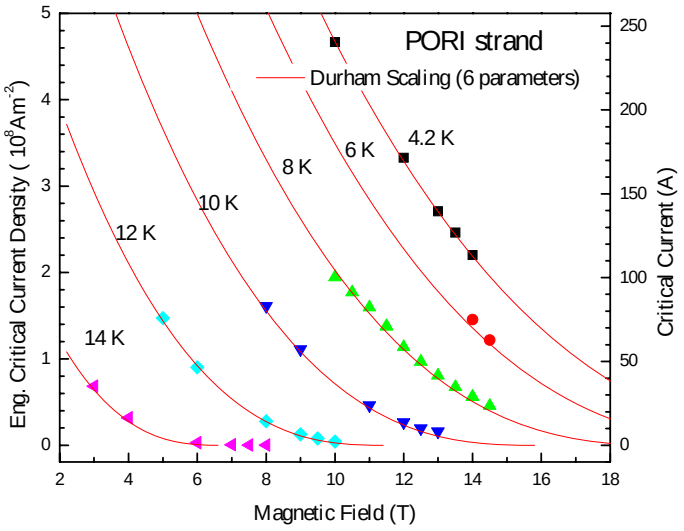

Figure 9. Engineering critical current density (and critical current) as a function of magnetic field with temperature from 4.2 K to 14 K for PORI strand at zero applied strain. The red solid lines are provided by the Durham scaling law using 6 free parameters listed in table III.

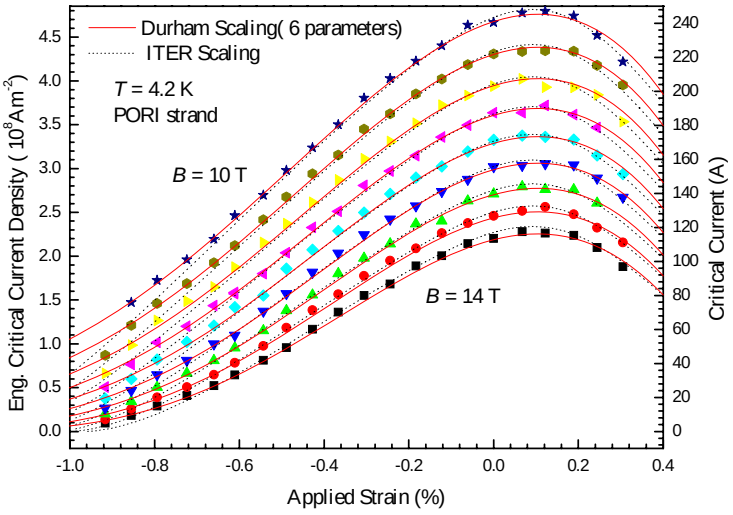

Figure 10. Engineering critical current density (and critical current) as a function of applied strain at 4.2 K and magnetic fields between 10 and 14 T for the PORI strand. The solid lines are provided by the Durham scaling law[20] using 6 free parameters listed in table III. The dotted lines are provided by the ITER scaling law[21] (parameters in table V).

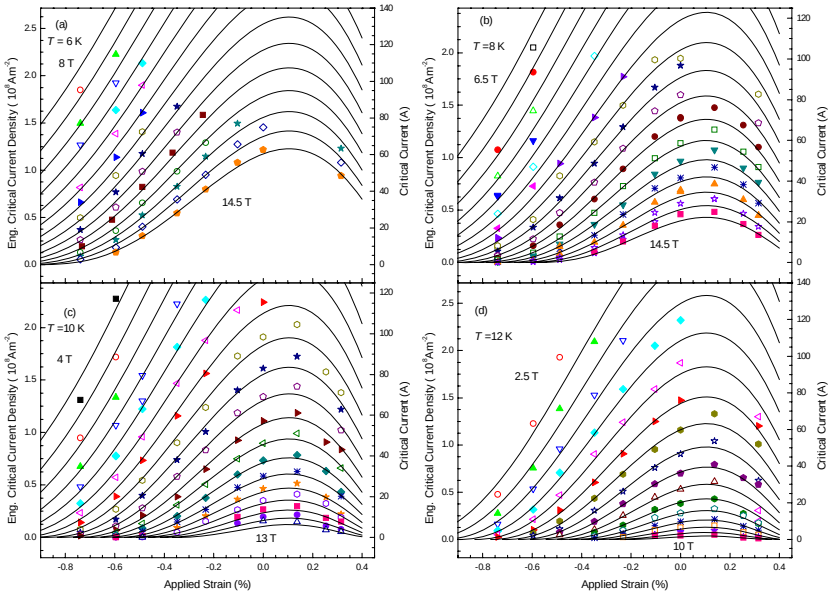

Figure 11. Engineering critical current density (and critical current) as a function of applied strain at magnetic fields shown. Panels (a) – (d) are at temperatures of 6 K, 8 K, 10 K and 12 K respectively. The lines are provided by the Durham scaling law using (6 free) parameters from table III

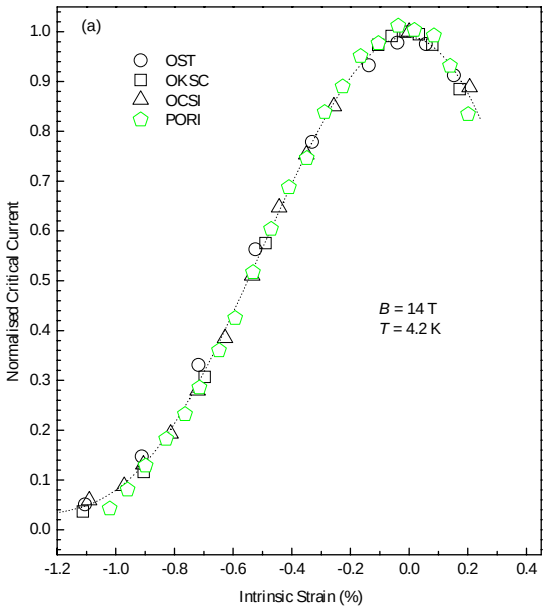

Figure 12. The normalized critical current at 4.2 K as a function of intrinsic strain for OST (I_{Max} = 219.6 A), OKSC (I_{Max} = 193.4 A), OCSI (I_{Max} = 149.6 A), and PORI (I_{Max} = 116.1 A) strands. The dotted line is a guide to the eye.

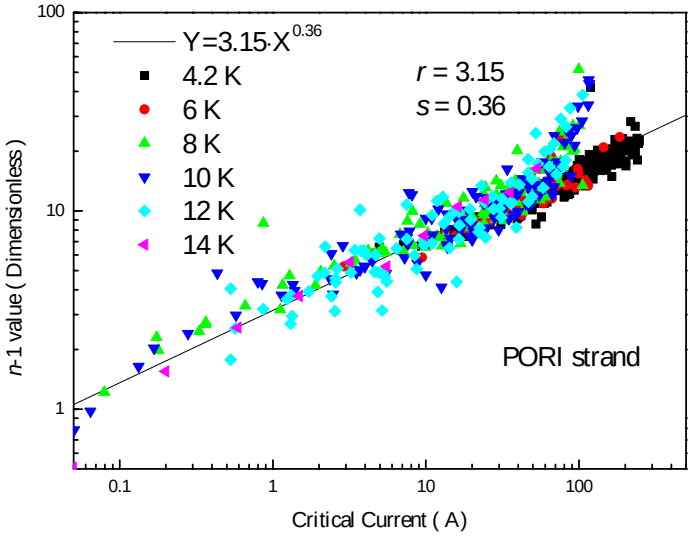

Fig. 13: The n-value obtained from fitting the experimental data to the equation $E = \alpha J^n$ over the range from 10 to 100 μVm^{-1}. Data are shown for the PORI strand by plotting n-1 as a function of critical current at T = 4.2 K, 6 K, 8 K, 10 K, 12 K and 14 K in different fields. The line show a fit made using equation (9), where r = 3.15 and s = 0.36.

3.3 Critical current and *n*-value parameterisation

3.3.1 Durham scaling law for critical current

The $J_C(B,T,\varepsilon)$ data at 10 μVm^{-1} are parameterised using the Durham scaling law[1], which involves the following relations:

$$J_C(B,T,\varepsilon_I) = A(\varepsilon_I)\left[T_C^*(\varepsilon_I)\left(1-t^2\right)\right]^2\left[B_{C2}^*(T,\varepsilon_I)\right]^{n-3} b^{p-1}(1-b)^q \quad (1)$$

$$B_{C2}^*(T,\varepsilon_I) = B_{C2}^*(0,\varepsilon_I)\left(1-t^v\right) \quad (2)$$

$$\left(\frac{A(\varepsilon_I)}{A(0)}\right)^{1/u} = \left(\frac{B_{C2}^*(0,\varepsilon_I)}{B_{C2}^*(0,0)}\right)^{1/w} = \frac{T_C^*(\varepsilon_I)}{T_C^*(0)} \quad (3)$$

$$\frac{B_{C2}^*(0,\varepsilon_I)}{B_{C2}^*(0,0)} = 1 + c_2\varepsilon_I^2 + c_3\varepsilon_I^3 + c_4\varepsilon_I^4, \quad (4)$$

$$\varepsilon_I = \varepsilon_A - \varepsilon_M, \quad (5)$$

where J_C is the engineering critical current density (the critical current divided by the total cross-sectional-area of the strand), ε_A is the applied strain, ε_I is the intrinsic strain, ε_M is the applied strain at the peak, T_C^* is the effective critical temperature, $t = T/T_C^*$ is the reduced temperature, B_{C2}^* is the effective upper critical field and $b = B/B_{C2}^*$ is the reduced field.

To date we have found that if comprehensive data are available, a 13 free-parameter fit is best for engineering purposes. However in many cases, there is little loss of accuracy parameterising the strands if the number of free parameters is reduced to 9 and universal values of n = 2.5, v = 1.5, w = 2.2, u = 0 are used [1]. Recently we reported $J_C(B,T,\varepsilon)$ measurements made on 3 optimised advanced internal-tin Nb_3Sn strands in magnetic fields up to 28 Tesla in Grenoble where the upper critical fields were measured directly[20]. Based on those measurements, we proposed that for advanced strands a strain dependence for the normalised effective upper critical field of advanced strands at T = 0 is of the form[20]:

$$\frac{B^*_{C2}(0,\varepsilon_I)}{B^*_{C2}(0,0)} = 1 - 0.77462 \cdot \varepsilon_I^2 - 0.59345 \cdot \varepsilon_I^3 - 0.13925 \cdot \varepsilon_I^4 \quad (6)$$

Equations (1) – (3) and (6) lead to a $J_C(B,T,\varepsilon)$ scaling law for advanced internal-tin strands with just six free parameters[12,20].

3.3.2 ITER scaling law for critical current

The extensive data in this work has also been parameterised using a scaling law[21] proposed for characterising interlaboratory measurements of ITER strands. It has 9 free parameters and is of the form:

$$J_C(B,T,\varepsilon_I) = \frac{C}{B} s(\varepsilon_I)(1-t^{1.52})(1-t^2) b^p (1-b)^q \ . \quad (7)$$

where $s(\varepsilon_I)$ is a specified function of strain. This equation follows excellent work that explicitly incorporates the 3-dimensional nature of strain into the scaling law[22]. It effectively includes a 1/κ term[23] . This can be contrasted with the $1/\kappa^2$ found in the Durham scaling law which is consistent with experiment data[1], computational work [2] and theory[3]. The concerns about the 1/κ choice have been discussed previously [20].

3.3.3 *n*-value parameterization

The *n*-value is defined via the following relation:

$$E = \alpha J^n \quad (8)$$

where E is the electric field and J is the (engineering) current density. A tabulation of the $J_C(B,T,\varepsilon)$ and $n(B,T,\varepsilon)$ data for SMI-PIT strand and PORI strand can be found in the spreadsheets that accompany this report [24]. The *n*-value is commonly used as a 'quality index' for the superconducting materials[25-27,28,29]. The origin of the *n*-value in superconducting strands can be attributed to the distributions in the critical current and the flux-flow resistivity within the filaments [26-28,30-32]. In some simples cases, non-uniformity of the filaments can be the most important factor that determines the *n*-value [27,28,31,33], in others intrinsic effects are important[32]. Given the similar inverted quasi-

parabolic behaviour found for both *n* and the critical current as well as the experimental result that *n* approaches to 1 as I_C to zero, the relationship between *n*-value and the critical current is parameterised using the following modified power law [9],

$$n(B,T,\varepsilon_1) = 1 + r(T,\varepsilon_1)\left[I_C(B,T,\varepsilon_1)\right]^{s(T,\varepsilon_1)}. \quad (9)$$

The relation between *n* and the critical current is shown in Fig.7 and Fig. 13 where we find that $s(T,\varepsilon_1)$ is approximately a constant for all the temperatures and applied strains for these strands and $r(T,\varepsilon_1)$ only very weakly depends on the applied strain. These observations are consistent with previous work on different types of strands [9]. We conclude that detailed understanding of the connectivity between the superconducting regions and the low-resistivity normal regions will be required to provide further insight into *n*-values but that the general behaviour observed in Fig. 8 suggests that further progress should now be possible although it is beyond the scope this report.

3.3.4 Parameterisation of the SMI-PIT strand.

The limited $J_C(B,T,\varepsilon)$ data sets (cf. Figures 3a and 3b) for the SMI-PIT Nb_3Sn strand were parameterised using scaling laws with just 9 free-parameters. The parameters from the Durham Scaling law are given in table II (the four parameters in bold are not varied in the fitting procedure). Although $T_C^*(0)$ was not fixed during the scaling process, the derived value of $T_C^*(0)$ was similar to the generally accepted value for Nb_3Sn (17.5 K) [1]. The data were also parameterized using the official ITER scaling law and the free parameters are given in table IV. The RMS difference between the measured I_C and parameterized values is ~ 3 A for the Durham scaling law whereas the ITER scaling law gives ~ 4 A. The parameters obtained by limiting the fitting procedure only to the data obtained at 4.2 and 8 K are provided in tables III and V for the Durham scaling and ITER scaling respectively.

The average values of *r* and *s* derived from the *n*-value data for the PIT strand were 3.12 and 0.47 respectively.

p	q	n	v	w	u	ε_M (%)
1.1753	2.655	***2.500***	***1.500***	***2.200***	***0***	0.020
$A(0)$ ($Am^{-2}T^{3-n}K^{-2}$)	$T_C^*(0)$ (K)	$B_{C2}^*(0,0)$ (T)	c_2	c_3	c_4	
1.356×10^8	17.47	29.46	–0.6153	–0.5780	–0.3002	

Table II: Durham scaling law parameters for the SMI-PIT strand derived from variable strain, field and temperature data using 9 free-parameters. Data were obtained at 4.2, 8, 10, 12 and 14 K. The four parameters in bold were not varied in the fitting procedure. (RMS ~ 3.2 A)

p	q	n	v	w	u	ε_M (%)
1.1928	2.488	***2.500***	***1.500***	***2.200***	***0***	0.0239
$A(0)$ ($Am^{-2}T^{3-n}K^{-2}$)	$T_C^*(0)$ (K)	$B_{C2}^*(0,0)$ (T)	c_2	c_3	c_4	
1.261×10^8	17.46	28.90	–0.6180	–0.6053	–0.3373	

Table III: Durham scaling law parameters for the SMI-PIT strand derived from variable strain, field and temperature data using 9 free-parameters. Data fitting was limited to 4.2 and 8 K. The four parameters in bold were not varied in the fitting procedure. (RMS ~ 2.2 A)

p	q	C	C_{a1}	C_{a2}
2.149	4.520	1.233×10^{12}	60.9422	25.0876
$\varepsilon_{0,a}$ (%)	ε_M (%)	$B_{C20max}^*(0,0)$ (T)		$T_{C0max}^*(0)$ (K)
0.4069	0.0193	34.10		17.04

Table IV: The official ITER scaling parameters for the SMI-PIT strand derived from variable field, variable temperature and variable strain data – 9 free parameters. Data fitting was limited to 4.2, 8, 10, 12 and 14 K. (RMS ~ 4.1 A)

p	q	C	C_{a1}	C_{a2}
2.1255	4.330	1.089×10^{12}	66.0797	29.9961
$\varepsilon_{0,a}$ (%)	ε_M (%)	$B^*_{C20max}(0,0)$ (T)		$T^*_{C0max}(0)$ (K)
0.4716	0.0193	29.9961		16.87

Table V: The official ITER scaling parameters for the SMI-PIT strand derived from variable field, variable temperature and variable strain data – 9 free parameters. Data fitting was limited to 4.2 and 8 K alone. (RMS ~ 2.2 A)

3.3.5 Parameterisation of the PORI strand.

The $J_C(B,T,\varepsilon)$ data of PORI strand were parameterized using 6, 9 and 13 free-parameters in tables VI, VII and VIII [20]. The RMS values show that the 6 free-parameter scaling law can fit the data well. These scaling results are plotted graphically in Figs. 9, 10 and 11 as solid lines. The most accurate global fit to the data using 13 free-parameters is shown in Fig. 14. The official 9 free-parameters ITER fit is also shown in table IX – it fits the data with a relatively large error. We have also fitted the limited data sets obtained at 4.2 , 6 and 8 K using the 9 parameter Durham fit and the official ITER fit – these are shown in tables X and XI.

The average values of r and s derived from the n-value data for the PORI strand were 3.15 and 0.36 respectively.

Universal Values	c_2	c_3	c_4	n	ν	w	u
	-0.77462	***-0.59345***	***-0.13925***	***2.5***	***1.50***	***2.20***	***0***
$A(0)$ ($Am^{-2}T^{3-n}K^{-2}$)	$T^*_C(0)$ (K)	$B^*_{C2}(0,0)$ (T)	p	q	ε_M (%)		
3.644×10^7	16.63	30.01	1.0129	2.653	0.1044		

Table VI. Durham scaling law parameters for the PORI strand with 6 free parameters. Data were obtained at 4.2, 6, 8, 10, 12 and 14 K. The seven parameters whose values are given in bold were not varied in the fitting procedure. (RMS ~ 3.1 A)

p	q	n	ν	w	u	ε_M (%)
0.8858	2.50̃0	***2.500***	***1.500***	***2.200***	***0***	0.093
$A(0)$ ($Am^{-2}T^{3-n}K^{-2}$)		$T_C^*(0)$ (K)	$B_{C2}^*(0,0)$ (T)	c_2	c_3	c_4
2.976×10^7		16.64	30.25	–0.8530	–0.7429	–0.2418

Table VII: Durham scaling law parameters for the PORI strand derived from variable strain, field and temperature data using 9 free-parameters. Data were obtained at 4.2, 6, 8, 10, 12 and 14 K. The four parameters in bold were not varied in the fitting procedure. (RMS ~ 2.4 A)

p	q	n	ν	w	u	ε_M (%)
1.0437	2.780	2.500	1.407	1.853	-0.0676	0.0903
$A(0)$ ($Am^{-2}T^{3-n}K^{-2}$)		$T_C^*(0)$ (K)	$B_{C2}^*(0,0)$ (T)	c_2	c_3	c_4
3.739×10^7		16.85	31.44	-0.7746	-0.5935	-0.1393

Table VIII: Durham scaling law parameters for the PORI strand derived from variable strain, field and temperature data using 13 free-parameters. Data were obtained at 4.2, 6, 8, 10, 12 and 14 K. (RMS ~ 2.4 A)

p	q	C	C_{a1}	C_{a2}
0.4077	1.828	2.128×10^{10}	57.3785	12.9486
$\varepsilon_{0,a}$ (%)	ε_M (%)	$B_{C20max}^*(0,0)$ (T)		$T_{C0max}^*(0)$ (K)
0.2377	0.0917	30.00		16.02

Table IX: The official ITER scaling parameters for the PORI strand derived from variable field, variable temperature and variable strain data – 9 free parameters. Data obtained at 4.2, 6, 8, 10, 12 and 14 K were used in the fitting. (RMS ~ 3.1 A)

p	q	n	ν	w	u	ε_M (%)
0.7791	2.242	***2.500***	***1.500***	***2.200***	***0***	0.0945

$A(0)$ ($Am^{-2}T^{3-n}K^{-2}$)	$T_C^*(0)$ (K)	$B_{C2}^*(0,0)$ (T)	c_2	c_3	c_4
2.490×10^7	16.43	29.70	–0.8344	–0.7078	–0.2242

Table X: Durham scaling law parameters for the PORI strand derived from variable strain, field and temperature data using 9 free-parameters. Data were only used at 4.2, 6, and 8 K. The four parameters in bold were not varied in the fitting procedure. (RMS ~ 2.2 A)

p	q	C	C_{a1}	C_{a2}
0.3841	1.785	2.056×10^{10}	57.2202	13.3710

$\varepsilon_{0,a}$ (%)	ε_M (%)	$B_{C20max}^*(0,0)$ (T)	$T_{C0max}^*(0)$ (K)
0.2577	0.0938	30.00	15.71

Table XI: The official ITER scaling parameters for the PORI strand derived from variable field, variable temperature and variable strain data – 9 free parameters. Data fitting was limited to 4.2, 6 and 8 K. (RMS ~ 2.5 A)

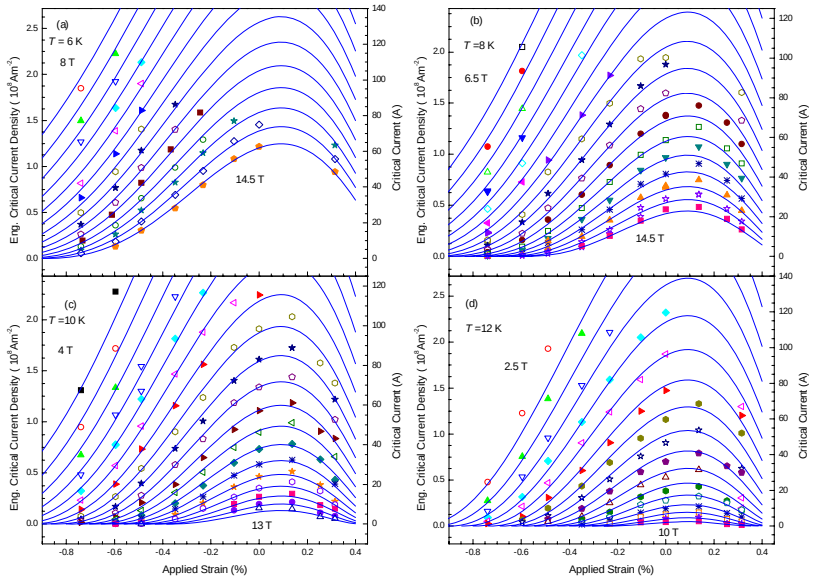

Figure 14. Engineering critical current density (and critical current) as a function of applied strain at magnetic fields shown. Panels (a) – (d) are at temperatures of 6 K, 8 K, 10 K and 12 K respectively for the PORI strand. The solid blue lines are provided by the Durham scaling law[20] using 13 free-parameters as given by table VIII.

4 STRAIN CYCLING TEST ON RRP STRAND

In a previous report EFDA05/1296 the engineering critical current density (J_C) of an RRP Nb_3Sn restacked-rod-process superconducting strand was reported as a function of magnetic field (B $\leq$ 28 T), applied axial-strain (-0.9 % $\leq$ ε_A $\leq$ 0.2 %) and temperature (4.2 K $\leq$ T $\leq$ 14 K). Although the strain tolerance of J_C was similar to other strands, the strain range over which J_C was reversible was limited in both tension and compression. Three samples were measured and found to be partially damaged on Tee-shaped Ti-alloy springs when the intrinsic strain (ε_I) was increased from -0.74 % to -0.97 % in compression and grossly damaged when ε_I was only 0.13 % in tension. The gross damage at low tensile strains (~ 0.13 %) have now been observed by a number of groups and precautions are implemented to ensure that when these RRP strands are used in high-magnetic-field systems they are not subjected to tensile strains. The scope of the work in this report is to investigate further, the partial damage observed in compression [13].

The procedure described in section 2 was followed and the voltage across six sections (A to F) were measured simultaneously during the course of the *I-V* measurements as a function of strain at 4.2 K. Figure 15 shows variable-strain I_C data for section A of the RRP Dipole strand at 4.2 K and 14 T as part of a strain cycling history. During the first three processes: the strain was applied from 0 to -0.47% and then changed back to 0; the strain was applied from 0 to -0.78% and then back to 0 and in the third process the strain was applied from 0 to -1.09% and then changed back to 0. The increment in the applied strain ($\Delta\varepsilon_A$) was ~ 0.07% during these three stages. During the fourth process the strain was applied from 0 to -1.25% (increments in strain ~ 0.30%) and then changed back to -1.09% (step ~ 0.07%). During the fifth process, the strain was then applied from -1.09% to -1.40% and then changed back to -1.09% with an increment in strain throughout of ~ 0.15%. The critical current data for one of the sections (Section A) is shown at 3 different fields in figures 15a, 15b, and 15c. We show the results during the third process for all the sections in Fig.16. Under uniaxial cycling, we do not expect complete reversibility for I_C because of the plastic deformation of some components of the Nb_3Sn strands[34]. However, it is clear that in contrast to previous results there is no clear evidence for partial damage in compression during these tests down to -1.40 % in any of the six sections.

After these five processes, we increased the applied compressive strain in steps of ($\Delta\varepsilon_A$) ~ 0.15% down to ~ -2.0% where the strand detached from the sample holder (spring). In these very high compressive strains, further work is required to obtain accurate data primarily because of the plastic deformation of the sample holder (spring).

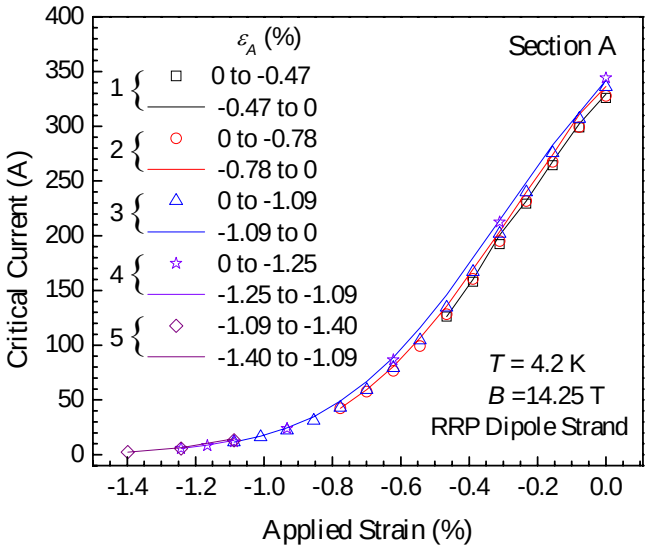

Figure 15a. Strain cycling test of RRP Dipole strand at 4.2 K and 14.25 T.

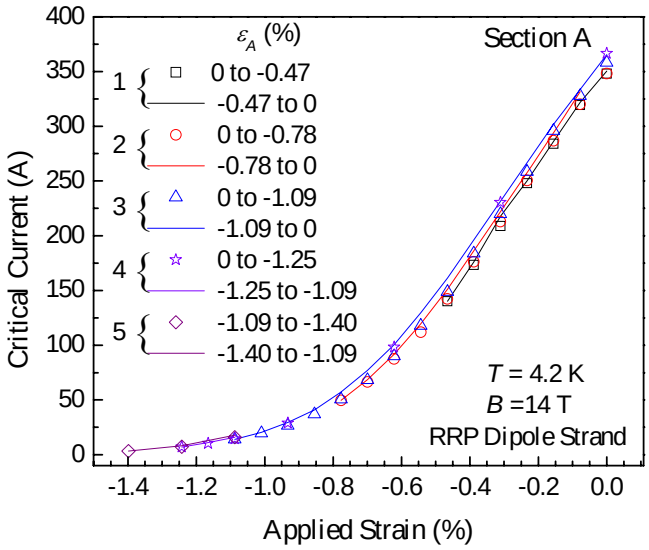

Figure 15b. Strain cycling test of RRP Dipole strand at 4.2 K and 14 T.

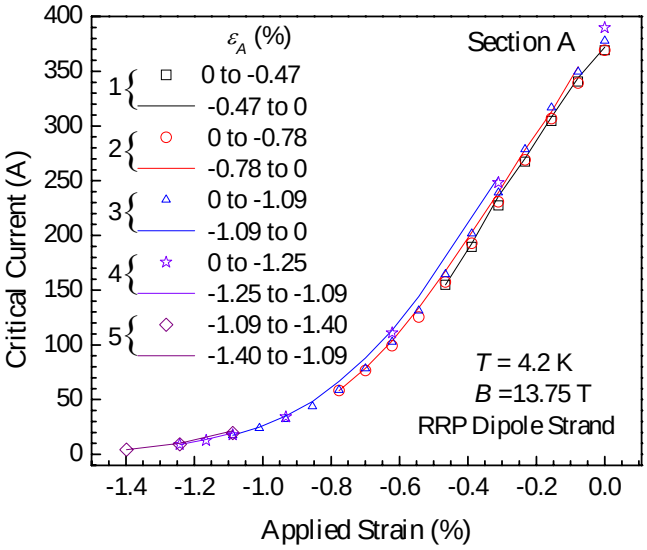

Figure 15c. Strain cycling test of RRP Dipole strand at 4.2 K and 13.75 T.

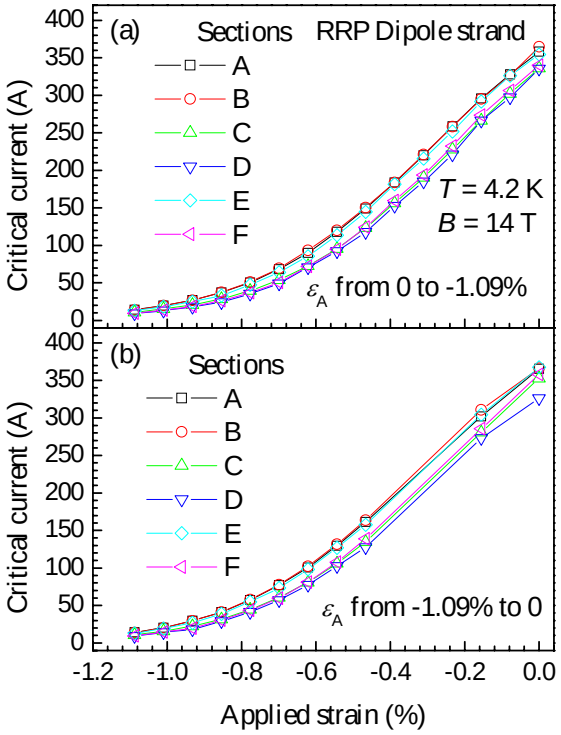

Figure 16. Homogeneity test of the critical current for six sections in the third stage with applied compressive strain (a) increasing and (b) decreasing.

5 DISCUSSION AND CONCLUSIONS

There is very limited data in the literature on PIT strands. Limited data taken at 4.2 K and 12 T [35] (in 2004) for the SMI-PIT strand carries about one-half of the current found in this report. The normalised strain sensitivity of both J_C (and I_C) (cf. Fig. 5) and the *n*-values (cf Fig. 8) are similar to other types of Nb_3Sn strands, although the absolute values of J_C are significantly higher (cf. Fig. 1) and *n*-values are about double those of other strands - see Fig.6. The very high I_C (non-Cu J_C ~ 2500A mm^{-2} at 4.2 K and 12 T)[6] and the acceptable effective diameter of the filaments (~ 50 um) open the possibility of using these strands in high energy Physics applications where high J_C is at a premium. The short heat-treatment times are also of value. However at present the production cost and the production methodology need to be improved to make these strands more commercially viable for fusion applications.

The early development of high J_C strands for magnet applications involved doping binary Nb_3Sn with elements such as Ta and Ti to increase the upper critical field (B_{C2}). Improvements of ~ 7 T were achieved at the expense of a stronger strain dependence for B_{C2} which can be explained using standard microscopic theory[1]. It follows that strands made using different fabrication routes, which lead to Nb_3Sn with different Sn content will have different reversible strain dependencies - consistent with the differences observed recently between bronze route strands and advanced internal-tin strands[1]. It is well-known that during the heat treatment of strands, the average Sn content and the morphology of the first Nb_3Sn that is formed is quite different to the average properties of the final Nb_3Sn layer[36]. This opens the possibility that even strands fabricated in a similar way may not have a similar strain dependence if the heat-treatment is significantly different. We report here [20] that although the short heat treatment time used for the PORI strand leads to significantly lower critical current density than optimized values, this strand has a similar strain dependence for J_C and *n* to advanced strands optimized for high J_C (see Figs 8 and 12). We also note that although J_C is much lower for the PORI strand than the optimized advanced strands in the literature, the B_{C2} values are similar [20]. Reliable comparisons of the (fitting) parameter T_C^* for different advanced strands are more problematic. Comparing fits to data on different strands, the type of fitting and quantity of data used at high temperature can affect T_C^*. Equally since the distribution of the critical temperature present (across the compositional variation) in a

filament can be large, a measurement of the critical temperature can be strongly dependent on how the measurement is made (e.g. resistive/percolative or magnetic/screening). Fortunately there is detailed thesis work by Naus [37] that suggests the critical temperature only changes by about 0.3 K between 60 h and 300 h in advanced internal-tin strands reacted at 650 ^{o}C. Hence we conclude that the long heat-treatment's primary effect, from the perspective of the reversible strain properties of J_C, is to increase the cross-sectional area of superconductor carrying the current without changing the intrinsic critical parameters very significantly and suggest that the normalized strain dependence observed in advanced internal-tin strands can be considered intrinsic to the composition of the Nb_3Sn layer that is produced.

The parameterization of the PORI data shows that a scaling law can accurately parameterize the $J_C(B,T,\varepsilon)$ data using just six free parameters. The data at the lowest reduced fields shows the largest deviation from the scaling law. This is because the reduced field dependence in the scaling law, which includes the parameters p and q, is a high-field expression (first proposed in the Fietz-Webb scaling law [38]). It is not sufficiently general to describe the field dependence of over the entire field range. In low fields non-linear terms (in the free-energy [39] and hence required in a pinning description of $J_C(B,T,\varepsilon)$ [40]) must be included for a more accurate parameterization. This scaling law is based on assuming a universal behaviour of the normalized effective upper critical field for the advanced internal-tin Nb_3Sn strands and provides a framework for comparing partial data sets from different laboratories. This work confirms the proposal [20] that one can consider the reversible strain dependence of the upper critical field to be intrinsic to the composition of the Nb_3Sn formed and hence to first order characteristic of the fabrication route used to produce the advanced PORI strand and insensitive to the details of the heat treatment.

We have completed extensive reversibility tests in the compressive applied strain for the RRP Dipole strand. Compressive strain cycling results are presented on the same rod-restack-process (RRP) strand investigated in a previous report (EFDA/05-1296) that considered reversibility limits in both tensile and compressive strain. The strong sensitivity of these strands to tensile strain has now been confirmed by other groups and is now considered a property of this type of strand alone. However in contrast to our previous results, no damage was observed in these measurements for compressive strains down to -1.4 %. The different behaviour in the strand may be due to inhomogeneity in

the strand, better handling, sample variations associated with pre-existing cracks (which have been observed in RRP strands elsewhere using electron microscopy) or use of rectangular Cu-Be sample holders rather than Ti-alloy when measuring this particular strand. We conclude that this strand is significantly different to other strands we have measured (cf the now established behaviour in tension), but recognise that further measurements (including detailed measurements, modelling and microscopy) are required to establish the underlying cause. Such investigations are beyond the scope of this report.

Durham University

APPENDIX I – Samples received

The samples received and documentation are outlined below. All documentation received with strands is Xeroxed, filed and is available from Hampshire (c.f. the links below). Samples in bold were those measured:

PIT SAMPLES

Letter from Vostner 070921 : \Documentation - samples received\071010 SMI Nb3Sn PIT B212\071010 SMI Strand document.pdf
Type: Ternary (NbTa) Nb3Sn PIT (SMI), billet B212. Configuration: High Jc strand (close to 3000 A/mm2 at 12 T, 4.2 K), Cu ratio 1,276. - Length: 30 m Diameter: 0.8 1 mm, Cr plated.

PORI SAMPLES:

1st PORI sample received was in fact a Dipole sample from Rossi (Not reported here).
DHL covering documentation: …\Documentation - samples received\060616 PORI (1st) is DIPOLE Nb3Sn DU2006-1\Luvata-pori Nb3Sn Strand.jpg

2nd PORI sample had tag NT8302 attached to the wire (Not reported here).
Letter from Vostner 070302: Type: Nb_3Sn internal tin (Luvata Finland), billet NT8302
Length: 20 m. Diameter: 0.813 mm, Cr plated. … \Documentation - samples received\070319 PORI (2nd) Nb3Sn BT8302\Heat Treatment - PORI NT8302 - EFDA.pdf
DHL covering note - Baldini: … \Documentation - samples received\070319 PORI (2nd) Nb3Sn BT8302\Heat Treatment - PORI NT8302 - EFDA.pdf

3rd PORI sample had no technical information. Tag attached to wire + DHL delivery note. \Documentation - samples received\071018 PORI DU2007-1\071018 PORI delivery note.pdf

RRP SAMPLE

The RRP strand was labelled as SPOOL 8712-2. Received by hand from Muzzi (MEM06) July 06.

APPENDIX II – Intermediate report

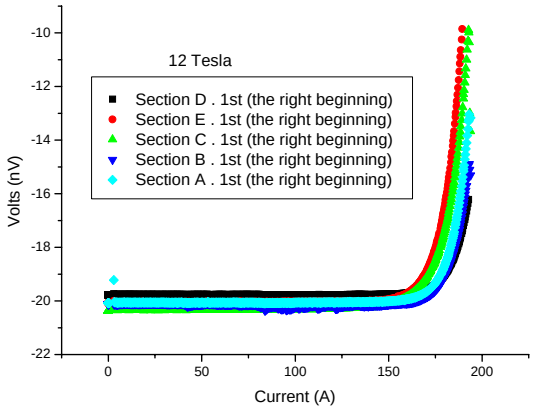

Figure 1 : The Pori sample measured at 12 Tesla and 4.2 K – zero applied strain.

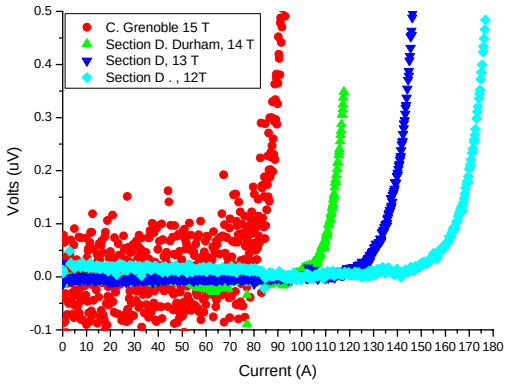

Figure 2 : The Pori sample measured at from 15 T to 12 Tesla and 4.2 K – zero applied strain (measured in Durham and Grenoble).

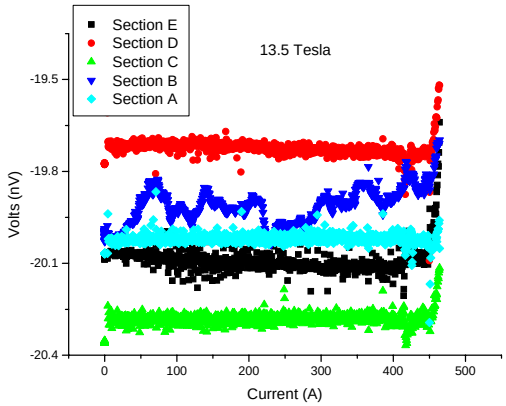

Figure 3: The SMI sample – measured in Durham at 13.5 Tesla.

Durham University

REFERENCES

1 D M J Taylor and D P Hampshire, "The scaling law for the strain dependence of the critical current density in Nb_3Sn superconducting wires," Supercond. Sci. Tech. **18**, S241-S252 (2005).

2 G Carty and D P Hampshire, "Visualising the mechanism that determines the critical current density in polycrystalline superconductors using time-dependent Ginzburg-Landau theory," Phys. Rev. B **77**, 172501 (2008).

3 E J Kramer, "Scaling Laws for Flux Pinning in Hard Superconductors," J. Appl. Phys. **44** (3), 1360-1370 (1973); E J Kramer, "Microstructure - Critical Current Relationships in Hard Superconductors," J. Elec. Mat. **4** (5), 839-879 (1975); D R Tilley and J Tilley, *Superfluidity and Superconductivity*, 3rd ed. (IOP publishing Ltd., Bristol, 1990).

4 S A Keys and D P Hampshire, in *Handbook of Superconducting Materials*, edited by D Cardwell and D Ginley (IOP Publishing, Bristol, 2003), Vol. 2, pp. 1297-1322.

5 A. Vostner and E. Salpietro, "Enhanced critical current densities in Nb_3Sn superconductors for large magnets," Superconductor Science & Technology **19**, S90-S95 (2006).

6 M. Di Michiel and C. Scheuerlein, "Phase transformations during the reaction heat treatment of power-in-tube Nb_3Sn superconductors," Superconductor Science & Technology **20**, L55-L58 (2007).

7 S Hong, M B Field, J A Parrell et al., "Latest improvement of Current Carrying Capability of Niobium Tin and Its Magnet Applications," IEEE Trans. Appl. Supercond. **16** (2), 1146-1151 (2006).

8 D O Welch, "Alteration of the superconducting properties of A15 compounds and elementary composite superconductors by nonhydrostatic elastic strain," Adv. Cryo. Eng. **26**, 48-65 (1980); A Godeke, B ten Haken, and H H J ten Kate, "The deviatoric strain description of the critical properties of Nb_3Sn conductors," Physica C **372 - 376**, 1295-1298 (2002); K C Lim, J D Thompson, and G W Webb, "Electronic density of states and T_C in Nb_3Sn under pressure," Phys. Rev. B **27** (5), 2781-2787 (1983).

9 D M J Taylor and D P Hampshire, "Relationship between the *n*-value and critical current in Nb_3Sn superconducting wires exhibiting intrinsic and extrinsic behaviour," Supercond. Sci. Tech. **18**, 297-302 (2005).

10 D P Hampshire, D M J Taylor, P Foley et al., Report No. DurSC0601, 2001.

11 D M J Taylor and D P Hampshire, Report No. EFDA-03-1126, 2005.

12 X F Lu and D P Hampshire, "The Magnetic Field, Temperature and Strain Dependence of the Critical Current of a Nb_3Sn Strand Using a Six Free-Parameter Scaling Law," IEEE Trans. Appl. Supercond. Submitted (2008).

13 X F Lu, S Pragnell, and D P Hampshire, "Small reversible axial-strain window for critical current in both compression and tension for a high performance Nb_3Sn superconducting strand," Appl. Phys. Lett. **91**, 132512 (2007).

14 D M J Taylor and D P Hampshire, "Properties of helical springs used to measure the axial strain dependence of the critical current density in superconducting wires," Supercond. Sci. Tech. **18**, 356-368 (2005).

[15] C R Walters, I M Davidson, and G E Tuck, "Long sample high sensitivity critical current measurements under strain," Cryogenics **26**, 406-412 (1986).

[16] N Cheggour and D P Hampshire, "A probe for investigating the effects of temperature, strain, and magnetic field on transport critical currents in superconducting wires and tapes," Rev. Sci. Instrum. **71** (12), 4521-4530 (2000).

[17] B L Brandt, D W Liu, and L G Rubin, "Low temperature thermometry in high magnetic fields. VII Cernox^{TM} sensors to 32 T," Rev. Sci. Instrum. **70**, 104-110 (1999).

[18] S A Keys, N Koizumi, and D P Hampshire, "The strain and temperature scaling law for the critical current density of a jelly-roll Nb_3Al strand in high magnetic fields," Supercond. Sci. Tech. **15**, 991-1010 (2002).

[19] A Vostner, Private communication. EFDA magnet experts workshop Barcelona (2007).

[20] X F Lu, D M J Taylor, and D P Hampshire, "Critical current scaling laws for advanced Nb_3Sn superconducting strands for fusion applications with six free parameters," Superconductor Science & Technology **21** (10), 105016 (2008).

[21] L Bottura, "$J_C(B,T,\varepsilon)$ Parameterization for the ITER Nb_3Sn Production," EFDA Intermediate Report, 1-23 (2008).

[22] B ten Haken, A Godeke, and H H J ten Kate, "The influence of compressive and tensile axial strain on the critical properties of Nb_3Sn conductors," IEEE Trans. Appl. Supercond. **5** (2), 1909-1912 (1995); W D Markiewicz, "Elastic stiffness model for the critical temperature T_C of Nb_3Sn including strain dependence," Cryogenics **44**, 767-782 (2004); W D Markiewicz, "Invariant formulation of the strain dependence of the critical temperature T_C of Nb_3Sn in a three term approximation," Cryogenics **44**, 895-908 (2004); W D Markiewicz, "Comparison of strain scaling functions for the strain dependence of composite Nb_3Sn superconductors," Superconductor Science & Technology **21**, 054004 (2008).

[23] A Godeke, B ten Haken, H H J ten Kate et al., "A general scaling relation for the critical current density in Nb_3Sn," Superconductor Science & Technology **19**, R100-R116 (2006).

[24] D P Hampshire, "Publication list and Excel files with the raw data on the group website," http://www.dur.ac.uk/superconductivity.durham/ (2008).

[25] P Bruzzone, "The index *n* of the voltage–current curve, in the characterization and specification of technical superconductors," Physica C **401** (1-4), 7-14 (2004).

[26] D P Hampshire and H Jones, "Critical current of a NbTi reference material as a function of field and temperature," Magnet Technology 9, 531-535 (1985).

[27] D P Hampshire and H Jones, "Analysis of the general structure of the *E-I* characteristic of high current superconductors with particular reference to a NbTi SRM wire," Cryogenics **27**, 608-616 (1987).

[28] W H Warnes and D C Larbalestier, "Critical current distributions in superconducting composites," Cryogenics **26**, 643-653 (1986).

[29] A K Ghosh, "*V-I* transition and *n*-value of multifilamentary LTS and HTS wires and cables," Physica C **401** (1-4), 15-21 (2004).

[30] J Baixeras and G Fournet, "Pertes par deplacement de vortex dans un supraconducteur de type II non ideal," J. Phys. Chem. Solids **28**, 1541-1547 (1967); H S Edelman and D C Larbalestier, "Resistive transitions and the origin of the n value in superconductors with a gaussian critical-current distribution," J. Appl. Phys. **74** (5), 3312-3315 (1993).

[31] W H Warnes, "A model for the resistive critical current transition in composite superconductors," J. Appl. Phys. **63** (5), 1651-1662 (1988); W H Warnes and D C Larbalestier, "Analytical technique for deriving the distribution of critical currents in a superconducting wire," Appl. Phys. Lett. **48** (20), 1403-1405 (1986).

[32] R Wördenweber, "Mechanism of vortex motion in high-temperature superconductors," Rep. Prog. Phys. **62**, 187 -236 (1998).

[33] D M J Taylor, S A Keys, and D P Hampshire, "*E-J* characteristics and *n*-values of a niobium-tin superconducting wire as a function of magnetic field, temperature and strain," Physica C **372**, 1291-1294 (2002).

[34] D M J Taylor and D P Hampshire, "Effect of axial strain cycling on the critical current density and *n*-values of ITER niobium-tin wires," Superconductor Science & Technology **401**, 40-46 (2004); M Suenaga and A F Clark, *Filamentary A15 Superconductors*. (1980).

[35] A Godeke, M Dhallé, A Morelli et al., "A device to investigate the axial strain dependence of the critical current density in superconductors," Rev. Sci. Instrum. **75** (12), 5112-5118 (2004); A. Nijhuis, Y. Ilyin, W. A. J. Wessel et al., "Critical current and strand stiffness of three types of Nb3Sn strand subjected to spatial periodic bending," Superconductor Science & Technology **19** (11), 1136-1145 (2006).

[36] J E Evetts, J R Cave, R E Somekh et al., "Characterisation of Nb_3Sn diffusion layer material," IEEE Trans. Magn. **17**, 360-363 (1981); J E Evetts and C J G Plummer, in *International Symposium on Flux Pinning and Electromagnetic Properties of Superconductors, Fukuoka, 1985*, edited by T Matsushita, K Yamafuji, and F Irie (Matsukuma, Fukuoka, 1985), pp. 146-151.

[37] M T Naus, University of Wisconsin - Madison, 2002.

[38] W A Fietz and W W Webb, "Hysteresis in superconducting alloys - Temperature and field dependence of dislocation pinning in niobium alloys," Phys. Rev. **178** (2), 657-667 (1969).

[39] E H Brandt, "Precision Ginzburg-Landau Solution of ideal vortex lattices for any induction and symmetry," Phys. Rev. Lett. **78** (11), 2208-2211 (1997).

[40] D Dew-Hughes, "Flux Pinning Mechanisms in Type II Superconductors," Philos. Mag. **30**, 293-305 (1974).